Proceedings of the Korean Nuclear Society Autumn Meeting
Seoul, Korea, October 1998

1D/2D ANALYSES OF THE LOWER HEAD VESSEL IN CONTACT WITH HIGH TEMPERATURE MELT

Jong-Eun Chang, Jae-Seon Cho, Kune Y. Suh, Chang H. Chung

Department of Nuclear Engineering, Seoul National University
San 56-1 Shinrim-dong, Kwanak-gu, Seoul, 151-742, Korea

ABSTRACT

One- and two-dimensional analyses were performed for the ceramic/metal melt and the vessel to interpret the temperature history of the outer surface of the vessel wall measured from typical Al_2O_3/Fe thermite melt tests LAVA (Lower-plenum Arrested Vessel Attack) spanning heatup and cooldown periods. The LAVA tests were conducted at the Korea Atomic Energy Research Institute (KAERI) during the process of high temperature molten material relocation from the delivery duct down into the water in the test vessel pressurized to 2.0 MPa. Both analyses demonstrated reasonable predictions of the temperature history of the LHV (Lower Head Vessel). The comparison sheds light on the thermal hydraulic and material behavior of the high temperature melt within the hemispherical vessel.

1. INTRODUCTION

The in-vessel cooling mechanism due to material creep and water ingression into the expanding gap between the debris and the vessel wall was found to explain the non-failure of the TMI-2 lower head. With the success of the modeling effort, a research program SONATA-IV (Simulation of Naturally Arrested Thermal Attack In Vessel) had been developed to thoroughly investigate this inherent nature of degraded core coolability inside the lower head by Suh et al. (1995, 1995a, 1995b, 1995c, 1996c), whose recent progress was reported by Kim and Kim (1997). In addition to the natural mechanism for heat removal, the program has also pioneered newly engineered concepts of in- and ex-vessel gap cooling structures for advanced reactor designs.

One- and two-dimensional analyses were performed for the ceramic/metal melt and the vessel to interpret the thermal behavior of the thermite and the vessel wall measured from typical LAVA tests during heatup and cooldown periods. The comparison of calculation and test results elucidates thermal hydraulic behavior of the high temperature melt within the hemispherical vessel. Analyses were also performed during the process of high temperature molten material relocation from the delivery duct down into the water in the test vessel pressurized to 2 MPa.

2. THEORICAL FRAMEWORK

2.1 The Continuum Debris Model

A two-region continuum debris model was developed by Suh and Henry (1994, 1996a, 1996b) to characterize the debris material and heat transport in the reactor lower plenum under severe accident conditions. In this model the debris bed is conglomerated into the oxidic pool and an overlying metallic layer. Steady-state relationships are used to describe the heat transfer rates, with the assessment of solid or liquid state, and the liquid superheat in the pool being based on the average debris temperature. Natural convection heat transfer from the molten debris pool

to the upper, lower and embedded crusts is calculated based on the pool Rayleigh number. The conduction heat transfer from the crusts is computed by the crust temperature profile. The downward heat flux is transferred to the lower part of the RPV lower head through a crust-to-RPV contact resistance and gap boiling. The sideward heat flux is transferred to the upper regions of the RPV lower head as well as the internal structures. The upward heat flux goes to the metal layer, particulated debris, water, or structures above.

2.2. Contact Resistance and Gap Boiling Heat Removal

In the TMI-2 accident, molten core material drained into the lower plenum and caused the RPV wall to reach temperatures of about 1100° C over a region of about 1 m in diameter. After reaching this temperature, the wall appears to have cooled rather quickly. One mechanism which could result in this rapid cooling is a limited amount of material creep of the RPV wall when these temperatures are reached. A model for representing this cooling process was proposed by Henry and Dube (1994) and Suh and Henry (1996a, 1996b).

Conceptually, when the steel wall is heated to temperatures where a significant creep rate could be anticipated, a gap could be expected to open between the wall and the debris, particularly if the debris is not tightly adhered to the RPV wall. Experimental observations were reported by Magallon et al. (1993), Hammersley and Henry (1993), Maruyama et al. (1996), and Henry et al. (1997), which supported that molten material poured through water does not adhere well to a steel wall. This development of a contact resistance may result from vaporization of the water in surface cavities. In the reactor system, relative movement between the wall and the heat generating material would occur when the RPV wall experiences material creep. With the increase in the gap, water may ingress between the debris crust and the RPV wall and effect cooling of the gap formed region.

3. ANALYSIS OF THERMAL TRANSIENT BEHAVIOR

3.1 One-Dimensional Thermal Behavior

3.1.1 Computational model description

One-dimensional thermal analysis is performed for typical LAVA-2 and LAVA-4 LHV temperature measurements at 0°. The LHV test section is a hemispherical carbon steel vessel which corresponds to 1/8 linear scale of the reactor vessel lower plenum. The inner diameter of the vessel is 50 cm and the thickness is 2.5 cm. The initial temperature of the molten alumina is assumed to be 2500 K and that of the LHV is 400 K. In the LAVA-4 test, the amount of the alumina is 30 kg. The grid meshes for the simplified one-dimensional analysis are 26 nodes in the alumina debris and 5 nodes in the carbon steel LHV.

For the simplified one-dimensional representation of alumina debris and the LHV shown in Fig. 1, the one-dimensional transient energy equation is represented as

$$\frac{\partial}{\partial t}(\rho h) = \frac{\partial}{\partial x}\left(\frac{k}{C_p}\frac{\partial h}{\partial x}\right) \tag{1}$$

The finite difference equation may be derived using the point scheme method

$$h_i = \frac{1}{\Delta x}\int_{i-1/2}^{i+1/2} h\,dx \tag{2}$$

where $i+1/2 = i + \Delta/2$, $i-1/2 = i - \Delta/2$

The right side is derived by the implicit method, while the material properties do not change for the time Δt.

$$\iint \frac{\partial}{\partial t}(\rho h)\,dt\,dx = \iint \frac{\partial}{\partial x}\left(\frac{k}{c_p}\frac{\partial h}{\partial x}\right)dx\,dt \tag{3}$$

$$\rho\Delta x(h_i^{p+1}-h_i^p)=\frac{k\Delta t}{c_p}\frac{h_{i+1}^{p+1}+h_{i-1}^{p+1}-2h_i^{p+1}}{\Delta x} \quad (4)$$

$$-Fo\,h_{i-1}^{p+1}+[2Fo+1]\,h_i^{p+1}-Fo\,h_{i+1}^{p+1}=h_i^p \quad (5)$$

where i=2,3,...,n-1, p = p-th time step, p+1 = (p+1)-th time step, Fo = $k\Delta t/\rho C_p(\Delta x)^2$ (Fourier number), the time step size Δt is fixed as 0.001 s, and the grid size Δx is 5 mm.

The matrix form is $\underline{A}x=b$, where $\underline{A}$ is a tridiagonal matrix. The enthalpy x is solved by the Gauss-Jordan elimination method.

The material properties for Al_2O_3 are given as

density (kg/m^3): 3965.0 @300K

thermal conductivity (W/m K): $85.537 - 0.22935\,T + 2.617e\text{-}4\,T^2 - 1.3755e\text{-}7\,T^3 + 2.7551e\text{-}11\,T^4$

specific heat (J/kg K): $-40.545 + 4.0217\,T - 5.000e\text{-}3\,T^2 + 2.88099e\text{-}6\,T^3$

porosity: $\varepsilon = 0.26017$

In the LAVA-4 test, for instance, the porosity was used to account for the difference between the volume of alumina with 100 % theoretical density (corresponding to calculated height of 0.106 m) versus the volume of alumina with the porosity (corresponding to the measured height of 0.125 m in the test). Also, the consequent properties of the simulant are weighted by the prosity(ε). Actually the porous media is not considered exactly. And the enchancement of a heat transfer area is neglected in the 1-D program. The properties were accordingly adjusted to accommodate for the pores within the debris assuming that the voids are filled with saturated steam.

The material properties for carbon steel are as

density (kg/m^3): 7854.0 @300K

thermal conductivity (W/m^2K): $58.527 - 1.5707e\text{-}2\,T - 2.3644e\text{-}5\,T^2 + 1.06925e\text{-}8\,T^3$

specific heat (J/kg K): $-711.0 + 6.27167\,T - 0.0107\,T^2 + 6.333e\text{-}6\,T^3$

In the above polynomial fit equations, the temperatures are given in K.

The upper boundary is covered with water compressed at 2.0 MPa in the tests. The lower boundary is exposed in the ambient air at 300 K. The heat transfer takes place in the film boiling regime at the upper boundary. Berenson's correlation (1961) is used accounting for the wave instability between the vapor and liquid phases as

$$h=0.425\left[\frac{h'_{fg}\rho_f(\rho_f-\rho_g)gk_f^3}{\sqrt{\frac{\sigma}{(\rho_f-\rho_g)g}}\mu_f\Delta T}\right]^{1/4} \quad (6)$$

where $h'_{fg}=h_{fg}+0.5c_p\Delta T$ with ΔT given by $T-T_{sat}$.

Film boiling heat transfer coefficients are employed when the temperature difference is above 100 K, while natural convection heat transfer coefficients are used below 20 K. The intermediate region is treated as a transition region switching from the film boiling to the single phase heat transfer. In addition, the radiation heat transfer is considered. The heat transfer coefficient in a gap formed between alumina and the LHV is represented as a gap conductance(k/δ) and the heat transfer coefficient with which the heat is bypassed through the gap between the alumina and LHV. The gap size is a pivotal parameter in this heat transfer mechanism. Starting with a 0.1 mm gap and comparing with 1.0 mm and 10 mm gaps, for instance, one can check on the sensitivity of the gap conductance in the overall heat transfer calculation. Through the deformed gap, the steam vapor leaves and the liquid water enters. In this one-dimensional program, it was simply represented by the heat transfer coefficient between the simulant and the heat sink, i.e. the steam vapor.

3.1.2 LAVA test simulation

In the LAVA-4 test, there forms initially a tiny gap of 1 μm which may expand up to 1 mm later on in the test.

The water trapped in the gap is vaporized and expelled. The water is assumed to be supplied immediately to satisfy the continuity inside the gap. The gap cooling heat transfer coefficients are varied in the film boiling regime. Sensitivity studies were performed to gain insight into the multi-dimensional analysis whose case results are summarized in Tables 1 through 5 and Figs. 2 through 6. Fig. 2 shows the effect of the initial gap size on the LHV thermal response. Note that the larger the initial gap, the slower the heatup rate of the LHV, which is well expected. Fig. 3 examines the effect of varying gap size deformation with the fixed initial gap of 1 μm. It appears that the LHV thermal response is rather insensitive to the values chosen given the heat transfer coefficient of 1000 W/m^2K. Fig. 4 demonstrates the LHV cooling rates with increasing heat transfer coefficients from 100 to 10000 W/m^2K, which is again well anticipated. In the one-dimensional code, the effect of the deformed gap size and that of the heat transfer coefficient cannot be considered at the same time. The increase of the gap size makes the heat transfer enhancement. Fig. 5 displays the effect of the timing for quenching the widened gap with rational performance. The above results for the LAVA-4 LHV temperature at 0° generally demonstrate that the simple one-dimensional analysis indeed provides with reasonable predictions for both the heatup and the cooldown periods.

Fig. 6 compares the computed and measured thermal histories for the LAVA-2 LHV at 0°. In this case rather accelerated heatup rates are calculated from this one-dimensional analysis in which the iron settles down underneath the alumina debris due to density difference thereby enhancing the conductive and convective (due to high superheat) heat transfer to the LHV wall at an early stage. However, in the actual LAVA-2 test, some degree of mixing between the iron and alumina might have taken place in the leading edge at the time of relocation to and contact with the LHV wall. Use of mechanical mixture properties could certainly improve the agreement of the computed curve with that measured for LAVA-2.

3.2 Two-Dimensional Thermal Behavior

3.2.1 FLUENT model application

Computational fluid dynamics code FLUENT 4.32 (1995) was used to simulate detailed transient two-dimensional thermal and flow distributions in the LAVA tests. FLUENT is a general-purpose computer program for modeling fluid flow, heat transfer, and chemical reaction. This code predicts the thermofluid phenomena by solving the conservation equations for mass, momentum and energy using a control volume based finite difference method. The unsteady turbulent two-dimensional basic equations for natural convection and heat transfer are solved using the SIMPLE algorithm and the power-law scheme in the curvilinear coordinates.

Numerical analyses are performed in a two-dimensional domain. The same material properties are consistently utilized for the alumina and iron debris as in the one-dimensional analysis. The calculation domain is limited to the molten pool and the LHV wall. It is assumed that the height of debris pool is 12.5 cm. The initial temperature of a molten debris pool is assumed to be 2500 K and that of the LHV is 400 K. The physical domain is of three-dimensional spherical configuration which is reduced to the rectangular coordinate using the grid transformation. The grid meshes are 36×36 nodes. The calculation domain and the physical grid domain are depicted in Fig. 7. The calculations were performed for the same LAVA-2 and LAVA-4 test results as were treated by the simple one-dimensional approach in the previous section.

The enthalpy method is used in FLUENT for modeling the phase change process. The energy equation is written in terms of the sensible enthalpy defined as

$$h = h_{ref} + \int_{T_{ref}}^{T} C_p dT \tag{7}$$

The total enthalpy is then expressed as

$$H = h + \Delta H \tag{8}$$

Therefore, the energy equation is written in terms of the total enthalpy as

$$\frac{\partial}{\partial t}(\rho h) + \frac{\partial}{\partial x_i}(\rho u_i h) + \frac{\partial}{\partial x_i}(\rho u_i \Delta H) = \frac{\partial}{\partial x_i}(k\nabla T) - \frac{\partial}{\partial t}(\rho \Delta H) \quad (9)$$

In Fig. 7 (a), W1 through W4 delineate the boundaries of the calculational domain. Table 6 presents the applied conditions to each boundary. W1 is the outer boundary surface of LHV which contacts with the atmosphere. This surface is exposed in the ambient air at 300 K. The surface boundary conditions are governed by the air natural convection and the radiation heat transfer. The air heat transfer coefficient h_{air} is assumed to be 50, ¥ å$_{ext}$ is the emissivity of the external surface and ¥ ô is the Stefan-Boltzmann constant. In the equations above, T_w and $T_{i\ Ä}$ represent the boundary surface temperature and the ambient air temperature, respectively. W2 is the gap and W3 is the same height location as the debris pool height. On the W2 surface, heat transfer is considered in terms of the CHF (critical heat flux) and the radiation heat transfer. T_{sat} is the saturation temperature at 2.0 MPa. The CHF is calculated from Monde et al.'s correlation (1982). The W3 boundary is given the conduction heat transfer. In Table 6, k_{vs} is thermal conductivity of the LHV and L is the distance between W3 and top of the LHV. W4 denotes the upper surface of the debris covered with water, whose boundary condition is given by the film boiling and radiation heat transfer to the water.

3.2.2 LAVA test simulation

In the LAVA-2 test the molten debris pool was stratified into a metal layer and an oxide layer on account of their density difference. The metal layer was located in the lower region in the test vessel. Unfortunately, however, the FLUENT code cannot calculate the multi-phase model and the phase-change model simultaneously. Therefore, the debris pool was assumed as homogeneous layer in this calculation. Fig. 8 shows a comparison of the LAVA-2 experimental data and the numerical calculation results for the temperature history in the LHV. The comparison spot is located in the 2 mm depth and 0 degree of the LHV outer surface. In Fig. 8 the solid line represents the experimental data and the dotted lines signify calculation results. The first dotted line denotes the result of the case where the gap heat transfer is not considered, and the second dotted line expresses the result of the case where that 1 μm gap is assumed between the debris and the LHV. In the first case, the computed maximum temperature is higher than the measured one by as much as 300 K. For the case of 1 μm gap, the calculated maximum temperature is slightly lower than the measured one. On the other hand, the cooling rate of both calculations is higher than that of the test. This is probably because this calculation assumed that the debris is homogeneously mixed whereas in the test the metal layer was mostly located in the lower region.

For the LAVA-4 test, only an Al_2O_3 oxide pool was considered in this calculation as in the one-dimensional analysis. Assumption that initially there is a tiny gap (1 μm) was consistently applied as in the one-dimensional analysis. After 300 s it is assumed that a uniform 1 mm gap is formed. The W2 boundary condition is derived from Monde et al.'s CHF correlation (1982). Note, however, that this correlation may not directly be applied to the situation at hand since geometric and operating pressure conditions are different in the LAVA test from the correlation condition. This required sensitivity study to be performed for the CHF heat transfer. These values were varied from 100% to 25%. Fig. 9 compares the LAVA-4 experimental data and the numerical calculation results for the temperature history in the LHV. The comparison spot is the same as in LAVA-2. Fig. 9 illustrates that as the heat transfer coefficient in gap decreases, the calculation result approaches the LAVA test result. Fig. 10 shows the numerical analysis results for (a) the flow pattern in the molten debris and (b) the temperature distribution at 90 s into the test. As shown in Fig. 10 (a), the debris pool solidifies from the upper boundary surface covered with water and from the gap between the debris and the LHV. The temperature varies fairly linearly within the crust region.

4. CONCLUSION

A gap resistance and boiling heat removal is employed for heat transfer between the debris bed, the RPV wall and steel structures, and most importantly the RPV-to-crust gap water. The proposed inherent cooling mechanism is consistent with the observations reported in the TMI-2 Vessel Inspection, and can explain why the RPV did not fail and why it experienced a comparatively rapid cooling after reaching temperatures of about 1100° C.

One- and two-dimensional analyses were performed for the ceramic/metal melt and the vessel to interpret the temperature history of the outer surface of the vessel wall measured from typical LAVA tests spanning heatup and cooldown periods. Both analyses demonstrated reasonable predictions of the temperature history of the LHV. The comparison sheds light on the thermal hydraulic and material behavior of the high temperature melt within the hemispherical vessel. In light of the simple, one-dimensional thermal analysis results and implications presented in this paper, detailed two-dimensional analytical investigations using the FLUENT, FIDAP and ABAQUS codes are under way to extend the current examination of the thermal behavior and creep deformation of the LHV.

ACKNOWLEDGMENT

The authors acknowledge the experimental data provided for this work by the Korea Atomic Energy Research Institute.

REFERENCES

Berenson, P.J.(1961), Film-boiling heat transfer from a horizontal surface, Journal of Heat Transfer, Vol. 83, p. 351.

FLUENT 4.32 User's Guide(1995), FLUENT Inc., Lebanon, NH, USA, January.

Hammersley, R.J. and R.E. Henry(1993), Experiments to address lower plenum response under severe accident conditions, EPRI Report No. TR-103389, Vols. 1 and 2.

Henry, R.E. and D.A. Dube(1994), Water in the RPV: a mechanism for cooling debris in the RPV lower head, presented at the OECD-CSNI Specialists Meeting on Accident Management, Stockholm, Sweden.

Henry, R. E. et al.(1997), An experimental investigation of possible in-vessel cooling mechanisms, CSARP Meeting, Bethesda, MD, USA, May.

Kim ,S. B. and H. D. Kim(1997), Recent progress in SONATA-IV project, OECD/NEA CSNI PWG-2, Third Meeting of TG-DCC, Rockville, MD, USA, May 9-10.

Magallon, D. and H. Hohmann(1993), High pressure corium melt quenching tests in FARO, OECD/NEA CSNI-FCI Specialists Meeting, Santa Barbara, CA, USA.

Maruyama, Yu et al.(1996), In-vessel debris coolability studies in ALPHA program, Proceedings of the International Topical Meeting on PSA'96, Park City, UT, USA, September.

Monde, M., H. Kusuda, and H. Uehara(1982), Critical heat flux during natural convective boiling in vertical rectangular channels submerged in saturated liquid, Journal of Heat Transfer, Vol. 104, pp. 300-303, May.

Suh, K.Y. and R.E. Henry(1994), Integral analysis of debris material and heat transport in reactor vessel lower plenum, Nuclear Engineering & Design, Vol. l5l, No. 1, pp. 203-221, November.

Suh, K.Y.(1995), SONATA-IV: Simulation Of Naturally Arrested Thermal Attack In Vessel - visualization study using Pyrex belljar and copper hemisphere heater, presented at the Cooperative Severe Accident Research Program (CSARP) Semiannual Review Meeting, Bethesda, MD, USA, May 1-5.

Suh, K.Y., C.K. Park and K.J. Yoo(1995a), CAMPFIRE-2000: Comprehensive Accident Management Program Featuring Innovative Research & Engineering for the Year 2000 and Beyond, presented at the OECD Specialist Meeting on Severe Accident Management Implementation, Niantic, CT, USA, June 12-14.

Suh, K.Y., C.K. Park and K.J. Yoo(1995b), In pursuit of naturally arrested thermal attack on reactor vessel during a severe accident, presented at the OECD-NEA CSNI PWG 4 & 2 Meetings, Issy-les-Moulineaux, France, September 26-29.

Suh, K.Y. and C.K. Park(1995c), SONATA-IV: Simulation Of Naturally Arrested Thermal Attack In Vessel, International Conference on Probabilistic Safety Assessment Methodology and Applications PSA'95, Seoul, Korea, November 26-30.

Suh, K.Y. and R.E. Henry(1996a), Debris interactions in reactor vessel lower plena during a severe accident - I. Predictive model, Nuclear Engineering & Design, Vol. 166, pp. 147-163, October.

Suh, K.Y. and R.E. Henry(1996b), Debris interactions in reactor vessel lower plena during a severe accident - II. Integral analysis, Nuclear Engineering & Design, Vol. 166, pp. 165-178, October.

Suh, K.Y. K.H. Bang and C.K. Park(1996c), Inherent cooling of debris in reactor vessel and its implications for severe accident management, International Conference on Probabilistic Safety Assessment and Management PSAM-III, Crete, Greece, June 24-28.

Table 1. Sensitivity test for the initial gap size in LAVA-4

Case of 1-D Code Set	Initial Gap Size [mm]	Deformed Gap Size [mm]	Heat Transfer Coefficient [W/m^{2}K]	Gap Deformation Time [s]
Case-1	0.0001	0.1	1.0×10^3	250
Case-2	0.001	0.1	1.0×10^3	250
Case-3	0.01	0.1	1.0×10^3	250

Table 2. Sensitivity test for the deformed gap size in LAVA-4

Case of 1-D Code Set	Initial Gap Size [mm]	Deformed Gap Size [mm]	Heat Transfer Coefficient [W/m^{2}K]	Gap Deformation Time [s]
Case-1	0.001	0.01	1.0×10^3	250
Case-2	0.001	0.1	1.0×10^3	250
Case-3	0.001	1.0	1.0×10^3	250

Table 3. Sensitivity test for the heat transfer coefficient in LAVA-4

Case of 1-D Code Set	Initial Gap Size [mm]	Deformed Gap Size [mm]	Heat Transfer Coefficient [W/m^{2}K]	Gap Deformation Time [s]
Case-1	0.001	0.1	1.0×10^2	250
Case-2	0.001	0.1	1.0×10^3	250
Case-3	0.001	0.1	1.0×10^4	250

Table 4. Sensitivity test for the gap deformation time in LAVA-4

Case of 1-D Code Set	Initial Gap Size [mm]	Deformed Gap Size [mm]	Heat Transfer Coefficient [W/m^{2}K]	Gap Deformation Time [s]
Case-1	0.001	0.1	1.0×10^3	150
Case-2	0.001	0.1	1.0×10^3	250
Case-3	0.001	0.1	1.0×10^3	350

Table 5. Sensitivity test for the gap and the heat transfer coefficient in LAVA-2

Case of 1-D Code Set	Initial Gap Size [mm]	Deformed Gap Size [mm]	Heat Transfer Coefficient [W/m^{2}K]	Gap Deformation Time [s]
Case-1	0.001	0.01	1.0×10^2	250
Case-2	0.001	1.0	1.0×10^3	250
Case-3	0.001	1.0	1.0×10^4	10

Table 6. Boundary conditions for LAVA-2 and LAVA-4 in the two-dimensional calculation

Boundary Surface	Boundary Condition
W1	$q'' = h_{CHF}(T_w - T_{sat}) + e_{ext}\, s\,(T_w^4 - T_{sat}^4)$
W2	$q'' = h_{CHF}(T_w - T_{sat}) + e_{ext}\, s\,(T_w^4 - T_{sat}^4)$
W3	$q'' = \dfrac{k_{vs}}{L}(T_w - T_{sat})$
W4	$q'' = h_{film}(T_w - T_{sat}) + e_{ext}\, s\,(T_w - T_{sat})$

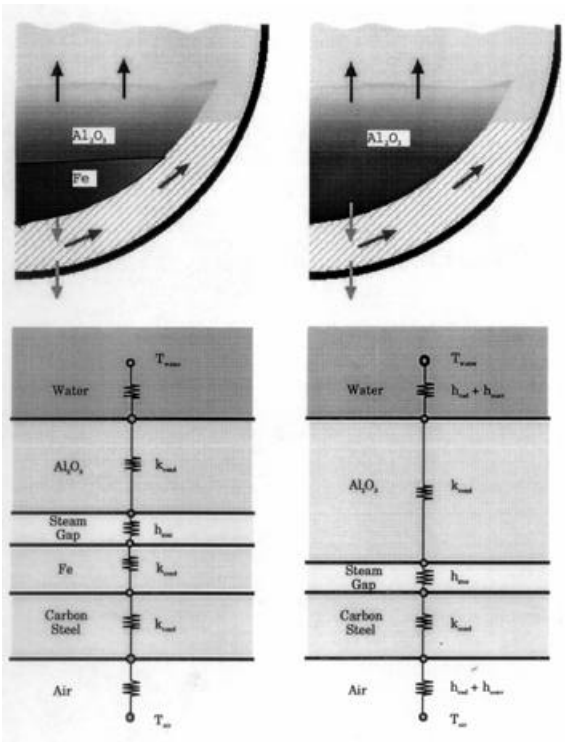

(a) LAVA-2 (b) LAVA-4

Fig. 1 One-dimensional representation of LAVA

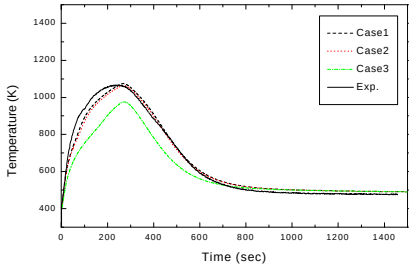

Fig. 2 Sensitivity test for the initial gap size in LAVA-4

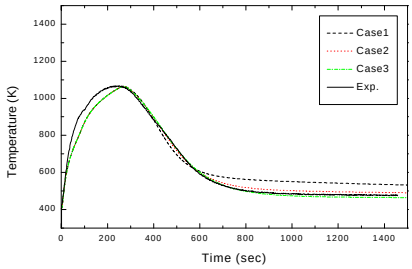

Fig. 3 Sensitivity test for the deformed gap size in LAVA-4

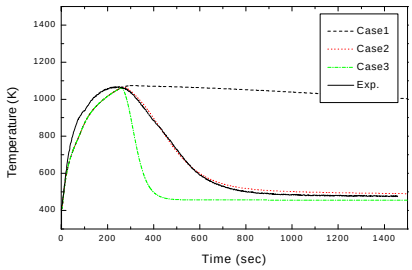

Fig. 4 Sensitivity test for the heat transfer coefficient in LAVA-4

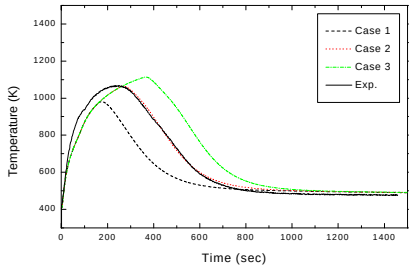

Fig. 5 Sensitivity test for the gap deformation time in LAVA-4

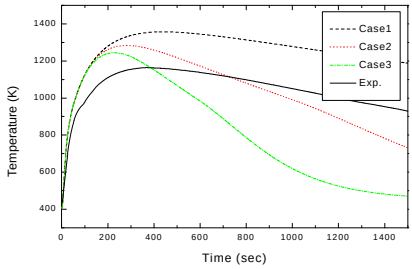

Fig. 6 Sensitivity test for the gap and heat transfer coefficient in LAVA-2

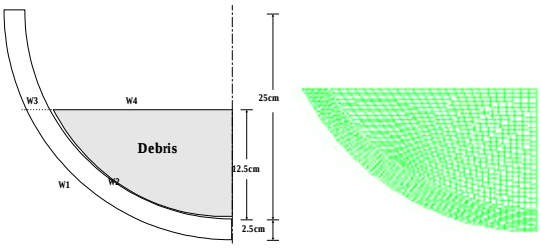

(a) Calculational domain (b) Physical grid

Fig. 7 Calculational domain and physical grid for LAVA simulation

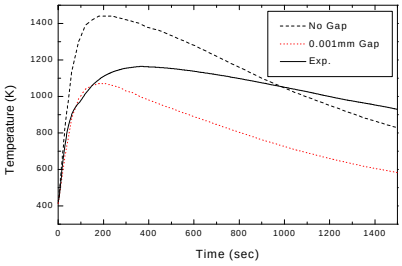

Fig. 8 Comparison of the temperature history with LAVA-2 test

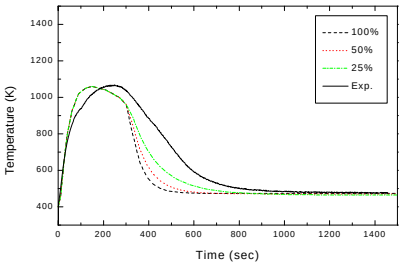

Fig. 9 Comparison of the temperature history with LAVA-4 test

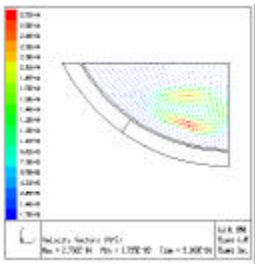

(a) Velocity vector

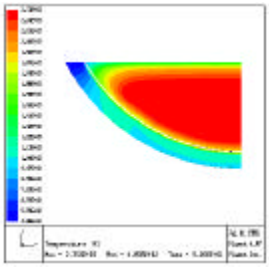

(b) Temperature profile

Fig. 10 FLUENT analysis results for the LAVA-4 test